

Hardware Implementation of Fano Decoder for PAC Codes

Amir Mozammel¹, *Student Member, IEEE*

Abstract—This paper proposes a hardware implementation architecture for Fano decoding of polarization-adjusted convolutional (PAC) codes. This architecture maintains a trade-off between the error-correction performance and throughput of the decoder by setting a strict limit on its search complexity. The paper presents analyses of the complexity, combinational delay, and latency of the proposed architecture. The performance of the proposed decoder is evaluated on FPGA and ASIC using Xilinx Nexys 4 Artix[®]-7 and TSMC 28 nm 0.72 V library, respectively. The PAC decoder can be clocked at 384.6 MHz and reach an information throughput of 9.34 MB/s at 3.5 dB signal-to-noise ratio for a block length of 128 and code rate of 1/2.

Index Terms—PAC codes, sequential decoding, Fano, polar codes, VLSI.

I. INTRODUCTION

POLARIZATION-adjusted convolutional (PAC) codes are a new class of error-correcting codes that have been shown to achieve near-optimum performance under sequential decoding [1, 2]. By combining ideas from channel polarization [3] and convolutional coding, PAC codes create an overall transform that achieves a performance near the information-theoretic limits at short block lengths. The goal of the present paper is to discuss the hardware implementation of Fano decoding for PAC codes. Fano decoding [4] is a well-known version of sequential decoding [5] that had been of interest in space communications before being superseded by Viterbi decoding [6]. To the best of authors' knowledge, combining sequential decoding with polar transform has never been implemented in hardware.

Under sequential decoding, PAC codes have variable search complexity. For practical hardware implementations of PAC codes, this may raise difficulties such as buffer overflow and/or data loss. In this paper, we study the complexity-performance trade-off in Fano decoding of PAC codes by introducing a method to limit the computational complexity. The proposed hardware implementation architecture for the PAC Fano decoder is also capable of employing the complexity-limiting method. We also study the hardware complexity, combinational delay, and latency of the proposed architecture, and, report the FPGA and ASIC implementation results.

The rest of this paper is organized as follows. In Section II, we provide a brief introduction to PAC coding. Section III studies Fano decoding of PAC codes in detail and provides preliminary definitions that are required for a better understanding of the proposed decoder. In Section IV, we introduce the hardware architectures for the main blocks of a PAC Fano decoder

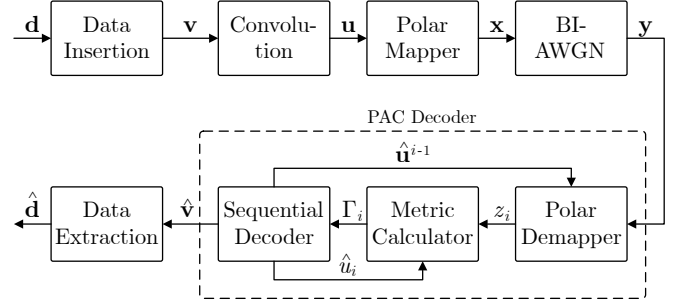


Fig. 1. PAC coding scheme.

and provide the complexity, delay, and latency analyses of each individual block. Implementation results of the proposed PAC Fano decoder are presented in Section V. Finally, Section VI concludes the paper and provides suggestions for future work.

Throughout this paper, all vectors are over the binary field $\text{GF}(2)$. We denote vectors by boldface letters. Unless otherwise noted, all logarithmic functions \log are in base 2. For any set $\mathcal{A} \subseteq \{1, 2, \dots, N\}$, we denote its complement by $\mathcal{A}^c = \{i : i \notin \mathcal{A}\}$. For any vector \mathbf{y} and set \mathcal{A} , $\mathbf{y}_{\mathcal{A}}$ denotes the subvector $(y_i : i \in \mathcal{A})$. For any vector \mathbf{y} , $\mathbf{y}^j = (y_1, y_2, \dots, y_j)$ and $\mathbf{y}_i^j = (y_i, y_{i+1}, \dots, y_j)$, $i \leq j$. We define a sign function $s(l)$ such that

$$s(l) := \begin{cases} +1, & \text{if } l \geq 0 \\ -1, & \text{otherwise.} \end{cases}$$

II. BACKGROUND ON PAC CODES

A PAC code is specified by four parameters $(N, K, \mathcal{A}, \mathbf{c})$, where N is the codeword length, K is the data length, \mathcal{A} is the data index set, and \mathbf{c} is the impulse response of convolution. The codeword length is constrained to be a power of two, $N = 2^n$ for $n \geq 1$, and data length K can be any integer between 1 and N . Fig. 1 shows the block diagram of the PAC coding scheme. The data insertion block receives a source word \mathbf{d} of length K and inserts it into a data carrier word \mathbf{v} of length N in accordance with the data index set \mathcal{A} such that $\mathbf{v}_{\mathcal{A}} = \mathbf{d}$ and $\mathbf{v}_{\mathcal{A}^c} = \mathbf{0}$. The bits that are fixed to zero are called *frozen*, whereas all the other bits are called *unfrozen*. The data carrier word \mathbf{v} goes through a convolution block, which is a rate one convolutional encoder with an impulse response \mathbf{c} . The resulting word \mathbf{u} goes through a polar mapper block, which is a rate one polar encoder. Then, the polarized codeword \mathbf{x} goes through a binary input additive white Gaussian noise (BI-AWGN) channel.

The author is with the Department of Electrical-Electronics Engineering, Bilkent University, Ankara TR-06800, Turkey (e-mail: a.mozammel@ee.bilkent.edu.tr).

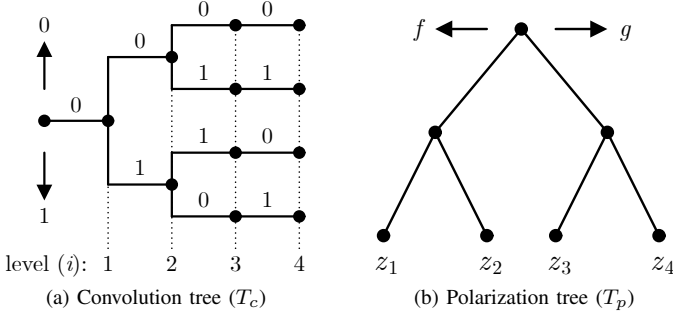


Fig. 2. PAC decoding trees.

At the receiver side, a polar demapper receives the channel output \mathbf{y} and calculates a log-likelihood ratio (LLR) vector $\mathbf{l} = (l_1, l_2, \dots, l_N)$ with

$$l_i = \ln \left(\frac{P(y_i | x_i = 0)}{P(y_i | x_i = 1)} \right).$$

Then, based on the prior estimates of convolution output $\hat{\mathbf{u}}^{i-1}$ made by the sequential decoder, it generates the unpolarized LLR value of the i th bit, z_i . A metric calculator block uses z_i to calculate the path metric Γ_i of node i based on the hypothesis $\hat{u}_i = 0$ or $\hat{u}_i = 1$, which is provided by the sequential decoder. Sequential decoding is performed on a code tree that will be explained in detail in Section III. Sequential decoder uses Γ_i to identify the correct path in the code tree, and consequently generates an estimate $\hat{\mathbf{v}}$ of \mathbf{v} . Finally, a data extractor extracts an estimate $\hat{\mathbf{d}}$ of \mathbf{d} from $\hat{\mathbf{v}}$ using $\hat{\mathbf{d}} = \hat{\mathbf{v}}_A$.

III. FANO DECODING OF PAC CODES

The decoding process of both convolutional codes and polar codes can be represented by a tree. Since PAC codes combine convolution and polar mapping, the decoding process of PAC codes consists of two trees: convolution tree and polarization tree, denoted by T_c and T_p , respectively. Fig. 2 shows an example of T_c and T_p for a PAC(4, 2, {2, 3}, 3) code, where $c = 3$ is in octal notation. A PAC code can be decoded using any sequential decoding algorithm, such as Fano and stack [7, 8], that traverses through T_c and searches for a correct estimate $\hat{\mathbf{v}}$ of \mathbf{v} . Whenever there is branching in a node at level i of T_c , the upper-branch corresponds to $\hat{v}_i = 0$ and the lower-branch corresponds to $\hat{v}_i = 1$. Each branch of T_c is labeled with corresponding convolution output \hat{u}_i .

The advantage of stack algorithm is that, unlike the Fano algorithm, it visits each node of T_c only once, and consequently performs fewer search operations. However, to perform the search operation on T_c , for every examined path, the stack algorithm requires to store partial data paths, corresponding path metrics, and convolution states in a stack. In contrast, the Fano algorithm only stores the current path $\hat{\mathbf{v}}^i$ and its path metric vector $\mathbf{\Gamma}^i$. To estimate the state of convolution, the Fano algorithm uses a convolutional encoder replica, from which the convolution output estimates \hat{u}_i are generated for each branch from node $i - 1$ to node i . Hence, the stack algorithm requires a larger memory size compared to the Fano algorithm. Additionally, the computational complexity of the

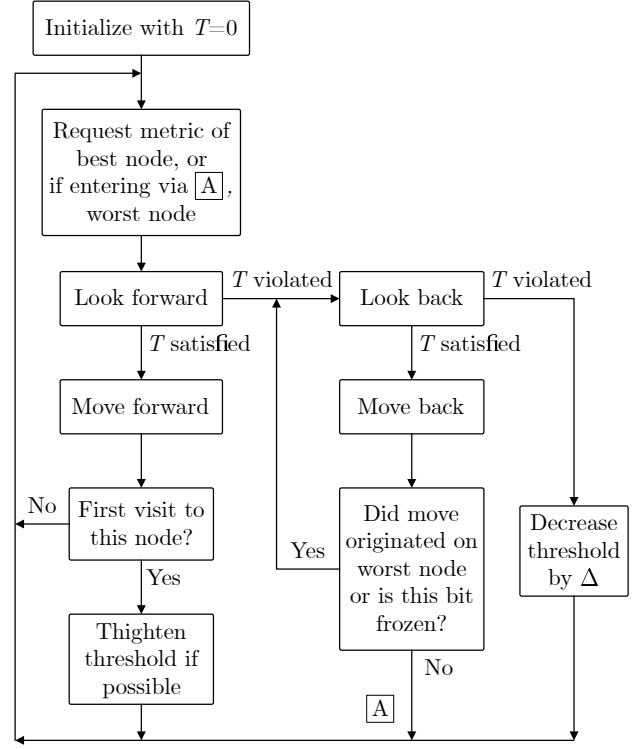


Fig. 3. Flow diagram of the PAC Fano decoder.

stack algorithm suffers from stack sorting operation. For these reasons, compared to the stack algorithm, the Fano algorithm is more practical for hardware implementations.

Fig. 3 shows the basic flow diagram of the Fano algorithm, which is modified to be suitable for decoding PAC codes. Fano algorithm is a depth-first search algorithm that uses a metric function to calculate the path metric vector $\mathbf{\Gamma} = (\Gamma_1, \Gamma_2, \dots, \Gamma_N)$ for finding the correct path on T_c . For PAC codes, the path metric is calculated using $\Gamma_i = \sum_{j=1}^i \gamma_j(\hat{u}_j)$, where $\gamma_j(\hat{u}_j)$ is the branch metric. For a BI-AWGN channel, the branch metric can be derived using [2] as

$$\begin{aligned} \gamma_j(\hat{u}_j) &= \gamma(\hat{u}_j, \mathbf{y} | \hat{\mathbf{u}}^{j-1}) \\ &= \log \frac{P(\mathbf{y} | \hat{\mathbf{u}}^j)}{P(\mathbf{y} | \hat{\mathbf{u}}^{j-1})} - b_j \\ &= \underbrace{1 - \log \left(1 + \exp(z_j)^{(2\hat{u}_j-1)} \right)}_{\alpha_j(\hat{u}_j)} - b_j, \end{aligned} \quad (1)$$

where z_j is the output of polar demapper, and b_j is a design parameter called bias. In the actual implementation of the PAC Fano decoder, we used the following design rule for the bias

$$b_j = \begin{cases} \rho, & \text{if } j \in \mathcal{A} \\ 0, & \text{otherwise,} \end{cases} \quad (2)$$

for some constant ρ .

To generate z_i , the polar demapper assigns the channel output LLR vector \mathbf{l} to the root of T_p and carries out the LLR values using two update rules called bit-node and check-node operations until reaching the leaf-node i . The bit-node and check-node operations are commonly denoted by f and

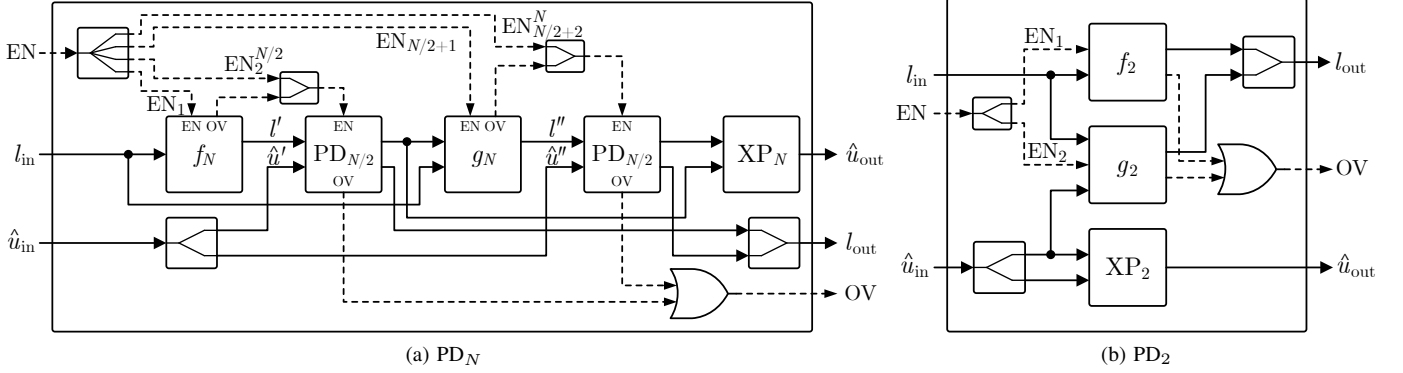


Fig. 4. Recursive architecture of polar demapper for (a) block length N and (b) block length two.

g , respectively. The f and g functions we used in the actual implementation of polar demapper are

$$f(l_1, l_2) = s(l_1)s(l_2) \min\{|l_1|, |l_2|\}, \quad (3)$$

$$g(l_1, l_2, \hat{u}) = l_2 + (1 - 2\hat{u})l_1. \quad (4)$$

As shown in Fig. 3, the Fano decoder moves forward or backward through T_c depending on whether the path metric satisfies or violates a running threshold T . Suppose the Fano decoder is currently at a node at level $i - 1$ of T_c . If the current bit is frozen, there is only one node forward, but if the current bit is unfrozen, there are two nodes forward. The Fano decoder request the metric of the best forward node (the one with higher Γ_i) and if the forward node's metric Γ_i satisfies the running threshold T , i.e., $\Gamma_i \geq T$, the algorithm moves forward. By moving forward, the bit pointer is incremented to i , the shift-register of convolutional encoder replica is shifted right by one, and the hypothesis \hat{v}_i corresponding to the taken branch is inserted into the shift-register. If a node is visited for the first time, the running threshold is tightened by a threshold increment Δ such that the new threshold satisfies $\Gamma_i - \Delta < T \leq \Gamma_i$.

If the running threshold is violated, i.e., $\Gamma_i < T$, the Fano decoder looks back at the previous node and if the previous node metric Γ_{i-2} satisfies the threshold T , the decoder moves back to that node. By moving back, the bit pointer is decremented to $i - 2$ and the shift-register of convolutional encoder is shifted left by one. When the Fano decoder moves back to a node j , there are three possible cases: (1) the bit j is frozen, i.e., $j \in \mathcal{A}^c$ and the decoder repeats the look back process, (2) the node j is reached from the worst node and the decoder repeats the look back process, and (3) the node j is reached from the best node and the decoder looks forward to the worst node. When the Fano decoder looks back and $\Gamma_{i-2} < T$, the algorithm decrements the threshold by Δ and looks forward to the best node of level i using the new threshold value.

The Fano decoder keeps repeating these steps until it reaches the last level of T_c , i.e., $i = N$, or a predefined termination criteria such as maximum searching time is satisfied. The search complexity of the Fano decoder is a random variable that highly depends on the noise magnitude. In this paper, we will denote the search complexity of the Fano decoder by a random variable Θ_i , which counts the number of

times the i th level of T_c is visited by the Fano decoder during a single decoding session.

IV. HARDWARE IMPLEMENTATION

As shown in Fig. 1, a PAC decoder consists of three main blocks: Polar Demapper, Metric Calculator, and Sequential Decoder. In this section, we will investigate the properties of these three blocks from a hardware implementation perspective. We will also provide a hardware architecture for each main block of PAC decoder and study the hardware complexity, delay, and latency of each individual block.

A. Polar Demapper

The task of a polar demapper is to depolarize the LLR values of channel output. The operation of the polar demapper is very similar to the one of successive cancellation (SC) decoder with the difference that, unlike SC decoder, the polar demapper does not make any hard decision at the leaf-nodes of T_c , i.e., it does not generate any bit-estimate output \hat{u}_i . Rather, it passes the LLR value z_i of the i th leaf-node of T_p to the metric calculator block. In short, a polar demapper can be considered and implemented as a soft-in soft-out SC decoder.

Despite the similarity in architecture, the timing schedule of polar demapper is different from the one of SC decoder in the sense that the polar demapper generates the leaf-node LLR values z_i one at a time, meaning that once it generated a leaf-node LLR value, it remains idle until another leaf-node LLR value is requested. Note that the next LLR value request may be for the immediate forward node or any other backward node. Hence, the polar demapper must be able to follow the Fano algorithm whenever it backtracks. Additionally, the polar demapper is required to output the leaf-node LLR values in natural order.

1) *Architecture*: Fig. 4a shows a recursive architecture of polar demapper for block length N (PD_N), which adopts the recursive structure of SC decoder described in [3]. We use a subscript along with the module name to indicate the number of inputs to that module. This architecture uses two polar demapper of size $N/2$ ($PD_{N/2}$), one f_N block, one g_N block, and one size- N XOR-and-PASS (XP_N) block. In this figure, l_{in} and l_{out} are the input and the output LLR values, and \hat{u}_{in}

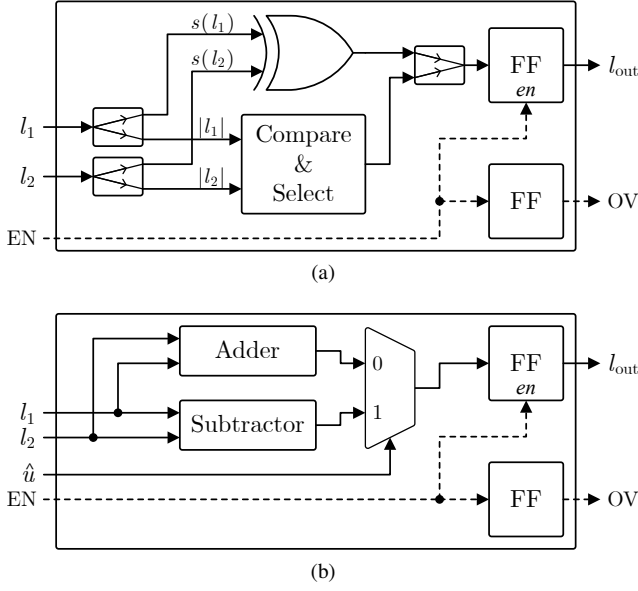


Fig. 5. Hardware diagrams of (a) f and (b) g blocks.

and \hat{u}_{out} are the input and the output bit estimates, respectively. In case of PD_N , l_{in} corresponds to the channel output LLR vector l and \hat{u}_{in} is the convolution output estimate \hat{u} . Also, for PD_N , the l_{out} corresponds to the leaf-node LLR values of T_c (z). Note that for PD_N , \hat{u}_{out} is redundant and has been shown for the sake of recursiveness.

The recursive architecture terminates at PD_2 for which the hardware design is shown in Fig. 4b. PD_2 uses one f_2 block, one g_2 block, and one XP_2 block. The f_2 and g_2 blocks implement (3) and (4), respectively. Fig. 5 shows the hardware diagrams of f_2 and g_2 blocks. The flip-flops (FF) are added to store the intermediate LLR values. The reason of using distributed registers instead of a unified storage such as random-access memory (RAM) is to reduce the routing complexity and delay. By doing so, every time a new leaf-node's LLR value is requested, the polar demapper does not have to start from scratch. Rather, it can start demapping from the least common ancestor of the current leaf-node and the previous leaf-node. The latter statement is only valid in the case of using a Fano decoder since it always moves from a current node either to its predecessor or to one of its immediate successors and it never jumps.

As noted before, a polar demapper needs to be able to move in forward and backward directions whenever the Fano decoder makes a forward or backward move, respectively. To obtain such a schedule, we added EN (enable) and OV (output-valid) control signals to f and g blocks. These control signals are depicted by dashed lines in Fig. 4 and Fig. 5. The signal EN is used for enabling the corresponding block and the signal OV goes high only when the output value of corresponding block is ready and valid. By concatenating these signals, one block can enable its following block whenever its output is ready.

To understand the timing schedule of polar demapper, consider a polar demapper for block length $N = 4$, for which the demapping trellis is shown in Fig. 6. Assume that the

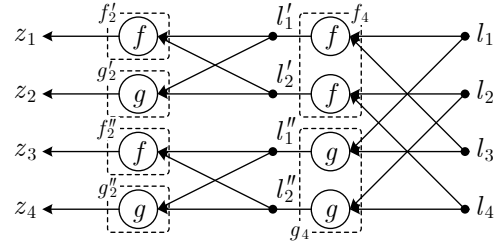


Fig. 6. Polar demapping trellis for $N = 4$.

Fano decoder is at the root of T_c and is exploring the first level of T_c , i.e., $i = 1$. Hence, it requests z_1 from the polar demapper by sending an enable signal to the f_4 block. The f_4 block outputs (l'_1, l'_2) and enables the f'_2 block. Finally, the f'_2 block generates z_1 . Next, the Fano decoder requests z_2 . Since l'_1 and l'_2 are already calculated and stored, to generate z_2 , the Fano decoder sends \hat{u}_1 to the polar demapper and enables the g'_2 block. The g'_2 block uses l'_1 , l'_2 , and \hat{u}_1 and generates z_2 . Similarly, to generate z_3 , the Fano decoder enables the g_4 block and the g_4 enables the f''_2 block, which in turn generates z_3 . Next, assume that the Fano decoder performs a backtracking and moves to the level $i = 1$ of T_c and requests z_2 . Same as before, since l'_1 and l'_2 are already available, to generate z_2 , the Fano decoder needs to send the updated value of \hat{u}_1 to the polar demapper and enable the g'_2 block. This procedure continues until the Fano decoder reaches the level $i = N$ (in this case $i = 4$) of T_c .

2) *Complexity*: Polar demapper's complexity can be expressed in terms of total number of comparators, adders, and subtractors used in the implementation. First, we estimate the number of comparators, which are used in the implementation of f function. As shown in Fig. 5, each f_2 block uses one comparator. We define c_N as the total number of comparators used in a polar demapper of size N . From Fig. 4b, we can see that the initial value of c_N can be taken as $c_2 = 1$. By observing Fig. 4a, we can obtain the recursive relationship for c_N as

$$c_N = \frac{N}{2} + 2c_{N/2} = \frac{N}{2} + 2 \left(\frac{N}{4} + 2c_{N/4} \right) = \dots$$

which has the following exact solution

$$c_N = \frac{N}{2} \log N.$$

Next, we estimate the number of adders and subtractors, which are used in the implementation of the g function. As shown in Fig. 5, each g_2 block uses one adder and one subtractor. Let a_N denote the total number of adders and subtractors used in a polar demapper of size N . It can be easily observed that $a_N = 2c_N$. Hence, we can obtain the total number of adders and subtractors as

$$a_N = N \log N.$$

Thus, the total number of basic logic blocks with similar complexities used for implementing the polar demapper is given by

$$c_N + a_N = \frac{3}{2} N \log N, \quad (5)$$

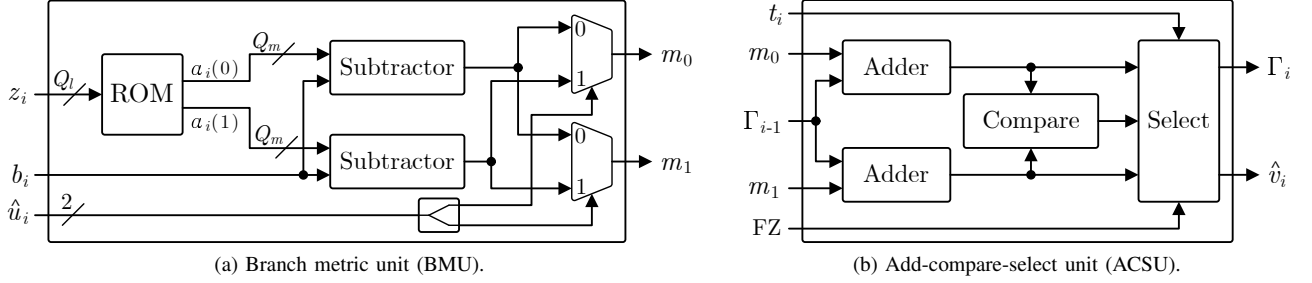


Fig. 7. Hardware diagram of the metric calculator block.

which shows the complexity of the polar demapper is $\mathcal{O}(N \log N)$.

Finally, we calculate the number of memory elements used in implementing the polar demapper. Let Q_l be the number of quantization bits for the LLR values. From Fig. 5, we realize that each f_2 and g_2 blocks requires Q_l flip-flops to store the LLR values and one flip-flop for passing the control signal. Although an f_4 or g_4 block consists of two parallel f_2 or g_2 blocks, respectively, by unifying the parallel control signals, we can reduce the number of FFs to $2Q_l + 1$. More generally, $(N/2)Q_l + 1$ number of FFs are required to implement an f_N or g_N block. We define s_N as the total number of FFs used in a polar demapper of size N . By observing Fig. 4a and taking the initial value of s_N as $s_2 = Q_l + 1$, we can obtain

$$\begin{aligned} s_N &= 2\left(\frac{N}{2}Q_l + 1 + s_{N/2}\right) \\ &= NQ_l + 2 + 2\left(2\left(\frac{N}{4}Q_l + 1 + s_{N/4}\right)\right) = \dots \end{aligned}$$

which has the following exact solution

$$s_N = (N \log N)Q_l + 2(N - 1). \quad (6)$$

3) *Combinational Delay and Latency*: We will approximately calculate the delay of polar demapper using combinational logic delays of each component forming the PD_N block. Referring to Fig. 4, we see that in each clock cycle, either an f block or a g block is activated. On the other hand, \hat{u}_{in} to \hat{u}_{out} path, which contains XP blocks, is an entirely combinational logic. If we denote the propagation delays of f_N , g_N , and XP_N by D_f , D_g , and D_{XP} , respectively, we can express the maximum combinational delay of the polar demapper as

$$D_{PD} = \max\{D_f, D_g, D_{XP}\}.$$

Using Fig. 5, we can express D_f and D_g as

$$\begin{aligned} D_f &= \delta_c + \delta_m, \\ D_g &= \delta_a + \delta_m, \end{aligned}$$

where δ_m , δ_c , and δ_a denote the delays of multiplexer, comparator, and adder/subtractor. Note that for the f block we assumed $\delta_x < \delta_c + \delta_m$, where δ_x is the delay of the XOR component. From Fig. 4, we observe that the value of D_{XP} depends on the index of the leaf-node i , for which the demapped value is requested from polar demapper, but can be approximated by its maximum value as $D_{XP} \approx \delta_x \log N$.

Next, we will examine the latency of the polar demapper. The number of clock cycles required for generating the LLR value of a leaf-node i (z_i) from channel output \mathbf{y}^N is defined as the latency of polar demapper and varies with respect to the value of i . The minimum latency occurs when the polar demapper generates z_i for the even leaf-nodes, i.e., for $i = 2, 4, \dots, N$, since for calculating the LLR values of these leaf-nodes only a single g_2 is required to be activated. On the other hand, the maximum latency occurs for the first node and node $i = \frac{N}{2} + 1$, since for these two cases the polar demapper needs to update the intermediate LLR values starting from the root of T_p tree down to the corresponding leaf-node. Hence, the latency of polar demapper is bounded by

$$1 \leq \text{Latency} \leq \log N.$$

B. Metric Calculator

The task of metric calculator block is to calculate and compare the path metrics for the two candidate nodes at level i of T_c , which are currently being examined by the Fano decoder, and, depending on the Fano decoder's choice, output the best or worst path metric Γ_i along with the corresponding decision \hat{v}_i . For the simplicity of discussion, we divide the metric calculator into two sub-blocks: branch metric unit (BMU) and add-compare-select unit (ACSU). The former calculates the branch metric $\gamma_i(\hat{u}_i)$ and the latter generates the path metric Γ_i and performs the compare and select operation.

1) *Architecture*: Fig. 7a shows the hardware diagram of BMU sub-block. Once the demapping process is performed by the polar demapper, a multiplexer (MUX) selects z_i from the l_{out} output of the polar demapper. This z_i is fed to the BMU sub-block along with the bias value b_i , and the convolution output estimates $\hat{u}_i = (\hat{u}_{i,0}, \hat{u}_{i,1})$, where $\hat{u}_{i,0}$ and $\hat{u}_{i,1}$ are the convolution output estimates for the two possible successor branches $\hat{v}_i = 0$ and $\hat{v}_i = 1$, respectively. In this figure, Q_l and Q_m denote the number of quantization bits for LLR and metric values, respectively. A synchronous dual-output read-only memory (ROM) is used to store the $\alpha_i(\hat{u}_i)$ values of (1) for 2^{Q_l} possible values of z_i . This module generates $\alpha_i(\hat{u}_i)$ for the two possible values of $\hat{u}_i = 0$ and $\hat{u}_i = 1$ for a given value of z_i . Then, the bias value of node i is subtracted from $\alpha_i(0)$ and $\alpha_i(1)$, resulting in $\gamma_i(0)$ and $\gamma_i(1)$, respectively. Finally, two 2-to-1 multiplexers select the proper values of γ_i in accordance with the values of $\hat{u}_{i,0}$ and $\hat{u}_{i,1}$. Consequently, the m_0 and m_1 outputs of BMU sub-block correspond to the

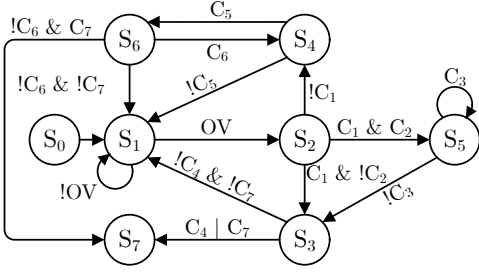


Fig. 9. Fano decoder state diagram.

of this random variable has a heavy-tailed nature such that a small fraction of codewords require a very large decoding complexity [9]. To eliminate the difficulties arising from the variable search complexity of the Fano decoder, we consider setting a strict limit on its search complexity by stopping the decoder and declaring a frame error when Θ_i exceeds a user-defined parameter θ_{\max} . To implement such a technique, we count the number of times the Fano decoder reaches each level of T_c by a forward move (denoted by θ_i) and use a RAM (NV-RAM) to store the values of θ_i for $i = 1, \dots, N$. After every forward move by the Fano decoder, if θ_i exceeds θ_{\max} , the decoding is terminated; a frame error flag is generated, all the blocks are reset, and a new received codeword \mathbf{y} is loaded to the input buffer. The justification of considering only forward moves and ignoring the visits by a backward or lateral move is provided in [10, p. 273].

Every Fano decoder has a central controlling unit that carries out the timing schedule by activating the corresponding blocks and providing their necessary inputs. We implemented this controlling unit using a finite-state machine (FSM). The FSM state diagram is shown in Fig. 9. The labels S_0 to S_7 represent the states of the Fano decoder. The state transitions happen according to the control signals C_1 to C_7 and OV output signal of the metric calculator block. In this figure, $!C$ denotes the logical complement of C , and the $\&$ and $|$ operators represent the logical AND and OR operations, respectively. The state names corresponding to S_0 to S_7 and expressions for generating the state transition signals C_1 to C_7 are listed in Table I. The equivalent circuitry for generating C_1 to C_7 is also shown in Fig. 8. The vector A indicates the frozen bits indices such that $A_i = 0$ if $i \in \mathcal{A}^c$, and $A_i = 1$ if $i \in \mathcal{A}$.

TABLE I
STATES AND STATE TRANSITION SIGNALS OF PAC DECODER.

Label	State	Signal	Expression
S_0	initialize	C_1	$\Gamma_i \geq T$
S_1	request metric	C_2	$\Gamma_{i-1} < T + \Delta$
S_2	look forward	C_3	$\Gamma_i \geq T + \Delta$
S_3	move forward	C_4	$i = N$
S_4	look back	C_5	$\Gamma_{i-2} \geq T$
S_5	tighten threshold	C_6	$t_i = 1$ OR $i \in \mathcal{A}^c$
S_6	move back	C_7	$\theta_i = \theta_{\max}$
S_7	stop	-	-

2) *Complexity*: As shown in Fig. 8, excluding the FSM block, the Fano decoder uses two adders, two subtractors, and eight comparators. Additionally, the FSM block uses one adder/subtractor for incrementing/decrementing the state

variable and two adders/subtractors for addressing the RAM blocks. The rest of the sub-blocks used inside the Fano decoder does not contain any adder/subtractor nor comparator. We can conclude that the complexity of the Fano decoder used inside a PAC decoder is $\mathcal{O}(1)$ independent of block-length N .

To calculate the column width of the M-RAM, we consider the worst case for which the metric calculator generates its maximum possible output value for all of the N nodes. The maximum metric magnitude that can be generated by metric calculator is $\max\{|\gamma_i|\} = 2^{Q_m-1} - 1$. Hence, assuming all the bits are unfrozen, $\rho = 1$, and considering one bit to represent the sign of metric value, the column width of M-RAM (W_M) can be approximated by

$$W_M \approx 1 + \lceil \log(N(2^{Q_m-1} - 1 + \rho)) \rceil \approx Q_m + n.$$

Also, the column width of NV-RAM, W_{NV} , can be approximated by $W_{NV} = \lceil \log \theta_{\max} \rceil$.

3) *Combinational Delay and Latency*: The adder/subtractor used for tightening/relaxing the threshold T , among the other components, dominates the combinational delay of the Fano decoder. The critical path starts from a register which stores T and goes through an adder/subtractor and returns to the same register. Hence, the total combinational delay of the Fano decoder can be expressed by $D_{\text{Fano}} = \delta_a$.

We define the latency of the Fano decoder as the number of clock cycles required for a single state to be executed. All the states have fixed latency except two states: request metric (S_1) and tighten threshold (S_5). The latency of S_1 depends on the latency of the polar demapper and the metric calculator for which we calculated the latency values in Section IV-A3 and Section IV-B3, respectively. The latency of S_5 depends on the value of the running threshold T prior to tightening as well as the path metric of forward node Γ_i . This latency can be expressed as $\lfloor \frac{\Gamma_i - T}{\Delta} \rfloor$.

The latency and search time of the PAC Fano decoder changes from one codeword to another, as well as from one signal-to-noise ratio (SNR) point to another. Because of this variable search complexity and variable latency, reporting a fixed throughput for a PAC Fano decoder is not possible. Rather, in the following, we report an average throughput which corresponds to the empirical mean of the number of decoded information bits per second over a given number of decoding trials for a given SNR value.

V. PERFORMANCE RESULTS

In this section, the implementation result of the proposed PAC Fano decoder is presented. The architecture is implemented both on FPGA and ASIC for block lengths of 2^6 , 2^7 , and 2^8 . With FPGA implementation, we investigate the FER performance of the decoder and study the number of lookup tables (LUTs) and flip-flops (FFs) used. We also calculate the average number of clock cycles required to decode a single information bit for a given SNR, which will be used to estimate the information throughput of the PAC decoder. With ASIC implementation, we study the area and power consumption as well as the maximum clock frequency which the decoder can be clocked at.

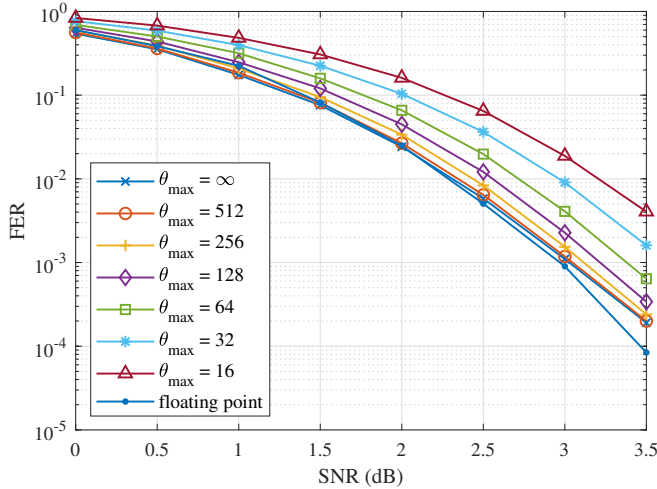


Fig. 10. FER performance of PAC decoder for $N = 2^7$ and different θ_{\max} values.

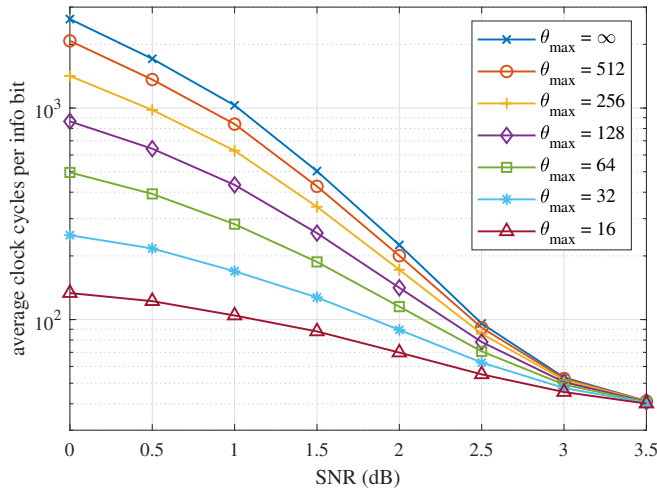


Fig. 11. Average number of clock cycles required for decoding one information bit.

In both FPGA and ASIC implementations, we used the following parameters: $R = 1/2$, $\Delta = 2$, $\rho = 1$, $Q_l = 6$, and $Q_m = 7$. Larger values of ρ result in better frame error rate (FER) performance but increase the search complexity of the PAC decoder. The choice of $\rho = 1$ is to maintain a good balance between FER performance and computational complexity. We chose the data set index \mathcal{A} according to the Reed-Muller (RM) scoring rule as explained in [1]. Based on our previous calculations for W_{NV} and W_M , we used $W_{NV} = 9$ for all three block lengths, and $W_M = 12, 13$, and 14 for block lengths of $2^6, 2^7$, and 2^8 , respectively.

TABLE II
FPGA IMPLEMENTATION RESULTS

N	LUT	FF	RAM (bits)
2^6	5626	3406	1344
2^7	13373	7385	2816
2^8	30038	16138	5888

A. FPGA Implementation Results

The proposed architecture for the PAC Fano decoder is tested on Xilinx Nexys 4 Artix[®]-7 (28 nm) FPGA at 100MHz clock frequency. Table II shows the place-and-route results of the proposed PAC Fano decoder on the FPGA. These results verify our complexity analysis of PAC Fano decoder specifying that the complexity of the decoder is $\mathcal{O}(N \log N)$. According to (6), 71, 76, and 79 percent of the total number of FFs listed in Table II are used to implement PD_{64} , PD_{128} , and PD_{256} , respectively.

Fig. 10 plots the FER performance of the decoder for block length of $N = 2^7$ and various values of θ_{\max} . Also shown in this figure is the FER performance of a software implementation of the PAC Fano decoder, which uses the same parameters as hardware implementation but unquantized (floating point) LLRs and metric values. The performance loss due to quantization is negligible. From this figure, we can see that as we increase the value of θ_{\max} , the FER performance of the decoder improves. As a matter of fact, by increasing the value of θ_{\max} , we allow the Fano algorithm to perform more search attempts, which results in decreasing the number of outage errors. For $\theta_{\max} = 512$ and beyond, the decoder performs as good as a PAC decoder with unlimited search complexity.

Fig. 11 shows the average number of clock cycles required for the decoder to decode a single information bit for the block length of $N = 2^7$ and various θ_{\max} values. Since the computational complexity of the Fano decoder is highly dependant on the severity of noise, the computational effort of the PAC Fano decoder decreases as the SNR increases. Also, as mentioned before, larger values of θ_{\max} allow the Fano decoder to explore more branches of the code tree, which results in a better FER performance but spending more clock cycles for decoding a single information bit. As shown in this figure, with $\theta_{\max} = 512$, the computational complexity of the decoder is very close to the one with $\theta_{\max} = \infty$. This is due to the heavy-tailed distribution of the PAC Fano decoder and that only a small fraction of codewords require a large computational complexity for being correctly decoded.

B. Post-Synthesis Results

Table III lists the post-synthesis results of the proposed PAC Fano decoder using Cadence[®] Innovus[™] Implementation System for the block lengths of $2^6, 2^7$, and 2^8 with TSMC 28 nm 0.72 V library. The decoders occupy area of 0.027, 0.062, and 0.134 mm^2 for the block lengths of $2^6, 2^7$, and 2^8 , respectively, from which approximately 28%, 54%, and 62% is allocated to the polar demapper, respectively. The number of standard cells listed in Table III verifies the hardware complexity of the PAC Fano decoder being $\mathcal{O}(N \log N)$. The decoders are capable of operating at 434.8, 384.6, and 357.1 MHz frequency consuming 8.59, 18.78, and 42.34 mW power for the block lengths of $2^6, 2^7$, and 2^8 , respectively. Comparing D_{ACSU} with D_{PD} and D_{Fano} , we realize that for the short block lengths the clock frequency of the PAC Fano decoder is limited by the combinational delay of the ACSU.

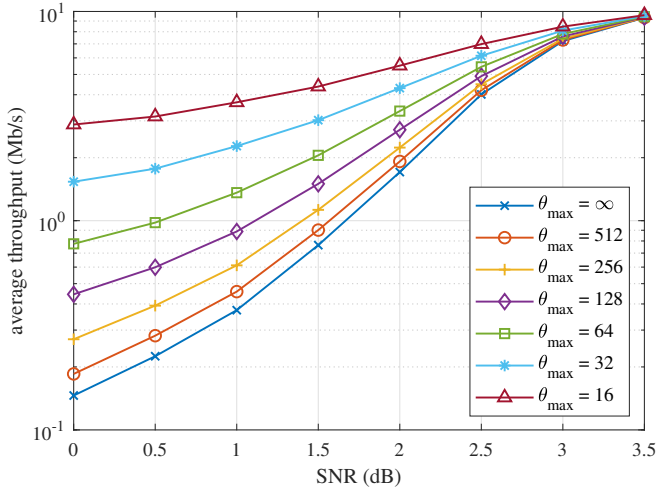


Fig. 12. Average THP of the PAC decoder at 384.6 MHz for different θ_{\max} values.

To estimate the average information throughput (THP) of the proposed PAC Fano decoder, we use the average number of clock cycles required to decode a single information bit, which can be obtained from Fig. 11, and the following relationship

$$\text{THP [bit/s]} = \frac{\text{Clock Frequency [cycle/s]}}{\text{Average Cycle [cycle/bit]}}$$

Fig. 12 plots THP of the proposed PAC Fano decoder for $N = 2^7$ and different values of θ_{\max} . The value of θ_{\max} has a significant effect on THP of the decoder at low SNR values, but as the SNR increases, this effect fades out to the point that all the THP curves overlap at 3.5 dB. At 0 dB SNR, using $\theta_{\max} = 16$, the THP can be boosted from 0.14 Mb/s to 2.88 Mb/s. Note that this THP boost comes at a cost of FER performance degradation, significantly at higher SNR values. The proposed decoder reaches an average information throughput of 9.34 Mb/s at 3.5 dB for block length of $N = 2^7$ and rate $R = 1/2$.

TABLE III
ASIC IMPLEMENTATION RESULTS

N	2^6	2^7	2^8
Technology	28 nm, 0.72 V		
Area [mm ²]	0.027	0.062	0.134
Number of Cells	17.03K	40.58K	89.29K
Power [mW]	8.59	18.78	42.34
Power Density [W/mm ²]	0.32	0.3	0.32
Frequency [MHz]	434.8	384.6	357.1

VI. CONCLUSION

In this paper, we proposed a hardware architecture for decoding the PAC codes using Fano algorithm. We provided analytical formulas for the complexity, combinational delay, and latency of each main block used in the implementation of the proposed PAC Fano decoder. Post-synthesis results showed that the proposed PAC decoder is capable of providing an information throughput of approximately 9.34 Mb/s at 3.5 dB SNR with a power consumption of 18.78 mW for a 28 nm 0.72 V technology for block length of 2^7 and rate $R = 1/2$.

Because of their high computational complexity, PAC codes suffer from limited throughput. At 3.5 dB SNR value, the decoder requires approximately 41 clock cycles on average for decoding one information bit for a PAC code of block length 2^7 and rate $1/2$. We introduced a technique to maintain a trade-off between the error-correction performance and the decoding complexity by limiting the maximum number of visits to each level of the code tree. Simulation results showed that this technique reduces the average computational complexity of the PAC Fano decoder at a cost of marginally sacrificing error-correction performance. This computational complexity reduction is significant at low SNR values.

Even though the throughput is limited, because of their extreme error-correction performance, PAC codes could be favorable for cases where reliable communication is more important than throughput. PAC codes use a very simple encoder which concatenates a rate one convolution and a rate one polar transform. Because of this simple structure of encoding, one of the potential use cases of PAC codes could be Internet of Things (IoT) for which a reliable communication and moderate throughput is of great interest.

Since the throughput of the decoder is limited by the combinational delay of ACSU sub-block of the metric calculator, as a future study, the throughput of the decoder can be increased by using an alternative design for the ACSU sub-block with a lower combinational delay. Among other things, the number of quantization levels plays an important role on the computational complexity of the Fano decoder [11, p. 369]. In this paper, the specified choices for the number of quantization levels for LLR and metric values, $Q_l = 6$ and $Q_m = 7$, were to minimize the area and obtain a reasonable FER performance. The optimization of computational complexity of sequential decoding of PAC codes subject to the number of quantization levels is yet to be investigated.

REFERENCES

- [1] E. Arıkan, "From sequential decoding to channel polarization and back again," *arXiv preprint arXiv:1908.09594*, 2019.
- [2] —, "Polarization adjusted convolutional codes," *submitted to IEEE Comm. Letters*, 1 Oct. 2020.
- [3] —, "Channel polarization: A method for constructing capacity-achieving codes for symmetric binary-input memoryless channels," *IEEE Transactions on Information Theory*, vol. 55, no. 7, pp. 3051–3073, 2009.
- [4] R. M. Fano, "A heuristic discussion of probabilistic decoding," *IEEE Transactions on Information Theory*, vol. 9, no. 2, pp. 64–74, 1963.
- [5] J. M. Wozencraft, "Sequential decoding for reliable communication," Research Laboratory of Electronics, MIT, Cambridge, Tech. Rep., 1957.
- [6] A. Viterbi, "Error bounds for convolutional codes and an asymptotically optimum decoding algorithm," *IEEE transactions on Information Theory*, vol. 13, no. 2, pp. 260–269, 1967.
- [7] K. Zigangirov, "Some sequential decoding procedures," *Problemy Peredachi Informatsii*, vol. 2, no. 4, pp. 13–25, 1966.

- [8] F. Jelinek, "Fast sequential decoding algorithm using a stack," *IBM journal of research and development*, vol. 13, no. 6, pp. 675–685, 1969.
- [9] M. Moradi, A. Mozammel, K. Qin, and E. Arıkan, "Performance and complexity of sequential decoding of pac codes," *submitted to IEEE Comm. Letters*, 19 Oct. 2020.
- [10] R. G. Gallager, *Information theory and reliable communication*. New York: Wiley, 1968, vol. 2.
- [11] A. J. Viterbi and J. K. Omura, *Principles of digital communication and coding*. Courier Corporation, 2013.